Differentially altered Ca^{2+} regulation and Ca^{2+} permeability in Cx26 hemichannels formed by the A40V and G45E mutations that cause keratitis ichthyosis deafness syndrome

Helmuth A. Sánchez,[1] Gülistan Meşe,[2] Miduturu Srinivas,[3] Thomas W. White,[2] and Vytas K. Verselis[1]

[1]Dominick P. Purpura Department of Neuroscience, Albert Einstein College of Medicine, Bronx, NY 10461
[2]Department of Physiology and Biophysics, Stony Brook University Medical Center, Stony Brook, NY 11794
[3]Department of Biological Sciences, State University of New York College of Optometry, New York, NY 10036

Mutations in *GJB2*, which encodes Cx26, are one of the most common causes of inherited deafness in humans. More than 100 mutations have been identified scattered throughout the Cx26 protein, most of which cause nonsyndromic sensorineural deafness. In a subset of mutations, deafness is accompanied by hyperkeratotic skin disorders, which are typically severe and sometimes fatal. Many of these syndromic deafness mutations localize to the amino-terminal and first extracellular loop (E1) domains. Here, we examined two such mutations, A40V and G45E, which are positioned near the TM1/E1 boundary and are associated with keratitis ichthyosis deafness (KID) syndrome. Both of these mutants have been reported to form hemichannels that open aberrantly, leading to "leaky" cell membranes. Here, we quantified the Ca^{2+} sensitivities and examined the biophysical properties of these mutants at macroscopic and single-channel levels. We find that A40V hemichannels show significantly impaired regulation by extracellular Ca^{2+}, increasing the likelihood of aberrant hemichannel opening as previously suggested. However, G45E hemichannels show only modest impairment in regulation by Ca^{2+} and instead exhibit a substantial increase in permeability to Ca^{2+}. Using cysteine substitution and examination of accessibility to thiol-modifying reagents, we demonstrate that G45, but not A40, is a pore-lining residue. Both mutants function as cell–cell channels. The data suggest that G45E and A40V are hemichannel gain-of-function mutants that produce similar phenotypes, but by different underlying mechanisms. A40V produces leaky hemichannels, whereas G45E provides a route for excessive entry of Ca^{2+}. These aberrant properties, alone or in combination, can severely compromise cell integrity and lead to increased cell death.

INTRODUCTION

The role of connexins in hearing has been established from genetic studies linking mutations in the *GJB2* gene, which encodes Cx26, to inherited forms of nonsyndromic and syndromic deafness (Kelsell et al., 1997; Gerido and White, 2004; Hoang Dinh et al., 2009; Lee et al., 2009). Mutations in the *GJB2* gene represent the most common cause of inherited recessive, nonsyndromic sensorineural deafness and can account for >80% of cases in some ethnic populations. Syndromic deafness linked to *GJB2* is accompanied by disorders such as keratoderma, hyperkeratosis, ichthyosis, and keratitis (Richard et al., 1998; Richard, 2000; Lee and White, 2009). Connexins form ion channels that classically assemble into gap junctions, which provide a direct signaling pathway between contacting cells. The gap junction or cell–cell channel is formed by two hexameric hemichannels or connexons that dock via their extracellular loop domains. Hemichannels, however, can function in the undocked configuration, thereby participating in signaling across the plasma membrane.

Mutations that cause deafness number >100 and are scattered throughout the Cx26 protein; at least 16 of these cause syndromic forms of deafness and generally cluster in the N terminus (NT) and the first extracellular loop (E1) domains (Lai-Cheong et al., 2007; Lee et al., 2009). In Cx46, Cx50, Cx32, and Cx26, the NT and E1 domains have been reported to be pore-lining domains and also contain elements essential for channel gating and regulation (Verselis et al., 1994, 2009; Oh et al., 2000; Purnick et al., 2000a,b; Kronengold et al., 2003b; Srinivas et al., 2005; Maeda et al., 2009). Missense mutations near the proximal portion of E1, such as G45E, A40V, and D50N, have been reported in cases of keratitis ichthyosis deafness (KID) syndrome, which is characterized by profound sensorineural hearing loss accompanied by

Correspondence to Vytas K. Verselis: vytas.verselis@einstein.yu.edu

Abbreviations used in this paper: KID, keratitis ichthyosis deafness; MTS, methanethiosulfonate; MTSES, 2-sulfonatoethyl-methanethiosulfonate; MTSET, 2-trimethylammonioethyl-methanethiosulfonate; NT, N terminus; SCAM, substituted cysteine accessibility method; TPEN, N,N,N′,N′-tetrakis(2-pyridylmethyl)ethylenediamine; WT, wild type.

The Rockefeller University Press $30.00
J. Gen. Physiol. Vol. 136 No. 1 47–62
www.jgp.org/cgi/doi/10.1085/jgp.201010433

vascularizing keratitis and erythrokeratoderma (Richard et al., 2002; Montgomery et al., 2004; Janecke et al., 2005). The G45E mutation has been linked to particularly severe cases of KID that can be fatal because of infections of skin lesions and septicemia (Janecke et al., 2005). It has been proposed that G45E, being a mutation that introduces a charged residue in an extracellular domain, may interfere with Ca^{2+} binding and regulation leading to so-called "leaky" hemichannels that could compromise cell integrity (Stong et al., 2006). Similarly, expression of G45E and A40V hemichannels in *Xenopus laevis* oocytes was shown to lead to rapid cell lysis (Gerido et al., 2007).

Here, we examined the properties of G45E and A40V hemichannels at macroscopic and single-channel levels and individually substituted cysteines at each position to evaluate accessibility using the substituted cysteine accessibility method (SCAM). We found that the A40V mutation imparts a substantial shift in regulation by extracellular Ca^{2+} consistent with a leaky hemichannel phenotype. However, we find that G45 is a pore-lining residue and that the principal effect of the G45E mutation is a substantial increase in Ca^{2+} permeability. Thus, these mutants may cause KID syndrome by different mechanisms, both of which can lead to increased cell death.

MATERIALS AND METHODS

Construction of Cx26 mutants

Human wild-type (WT) Cx26 was cloned into the BamHI restriction site of the pCS2$^+$ expression vector for functional studies in *Xenopus* oocytes. Mutant Cx26-G45E was prepared by site-directed mutagenesis using the gene splicing by overlap extension method (Horton et al., 1990) as previously described (Gerido et al., 2007). Mutant Cx26-A40V was directly amplified from patient genomic DNA as previously described (Montgomery et al., 2004). Site-directed mutagenesis to construct cysteine mutants was performed with the QuikChange Mutagenesis kit (Agilent Technologies) in accordance with the manufacturer's protocol using the WT connexin expression construct as a template. All constructs were verified by sequencing.

Exogenous expression of connexins

Expression of connexins in *Xenopus* oocytes, synthesis of RNA, preparation, and injection of oocytes have been described previously (Trexler et al., 1996, 2000). In brief, mRNA was prepared from appropriately linearized plasmid DNA with the mMessage mMachine SP6 RNA kits (Applied Biosystems) according to the manufacturer's protocol. The mRNA was purified using QIAquick PCR purification columns (QIAGEN). Each oocyte was injected with 50–100 nl of the mRNA solution. Injected oocytes were maintained at 16–18°C in a modified ND96 solution containing 100 mM NaCl, 2 mM KCl, 1 mM $MgCl_2$, 1.8 mM $CaCl_2$, 10 mM glucose, 10 mM HEPES, and 5 mM pyruvate, pH adjusted to 7.6.

For expression of connexins in mammalian cells, communication-deficient neuro-2A (N2A) cells were transiently transfected with A40V or G45E in the pIRES2-EGFP2 vector (Takara Bio Inc.) using Lipofectamine 2000 reagent (Invitrogen) as previously described (Meşe et al., 2008) with the exception that the calcium concentration in the tissue culture media was elevated to a final concentration of 3.2 mM with supplemental $CaCl_2$.

Electrophysiological recording and analysis

For recordings of macroscopic hemichannel currents, *Xenopus* oocytes were placed in a polycarbonate RC-1Z recording chamber (Warner Instruments) consisting of a slot-shaped chamber connected at opposite ends with inflow and outflow compartments. A suction tube was placed in the outflow compartment as well as agar bridges containing ground wires. Perfusion solutions consisted of 100 mM NaCl, 1 mM $MgCl_2$, and 10 mM HEPES, to which Ca^{2+} concentration was adjusted to desired levels. 0 Ca^{2+} solutions refer to nominal conditions in which no $CaCl_2$ was added. For reversal potential measurements of the Ca^{2+}-activated chloride currents elicited in oocytes expressing the G45E mutation, oocytes were voltage clamped to −50 mV and perfused with a solution consisting of 100 mM NaCl, 1 mM $MgCl_2$, 5 mM HEPES, and 0.2 mM $CaCl_2$ to promote hemichannel opening. Oocytes were then stepped to a series of voltages, starting with −60 mV in 10-mV increments. After the hemichannel current reached steady state during each voltage step, the oocytes were briefly exposed to a high Ca^{2+} (2 mM) solution to allow Ca^{2+} entry through open hemichannels and activation of the Ca^{2+}-activated chloride currents. Current amplitude was measured at the peak of the transient immediately after perfusion with 2 mM Ca^{2+}. This series was repeated in solutions in which KCl was replaced with K-aspartate. All recordings were obtained with a two-electrode voltage clamp (GeneClamp 500; Axon Instruments). Both current-passing and voltage-recording pipettes contained 1 M KCl. For patch clamp recordings of single hemichannel currents, *Xenopus* oocytes were manually devitellinized in a hypertonic solution consisting of 220 mM Na aspartate, 10 mM KCl, 2 mM $MgCl_2$, and 10 mM HEPES and were placed in the ND96 solution for recovery. Oocytes were then individually moved to a recording chamber (RC-28; Warner Instruments) containing the patch pipette solution, which consisted of 140 mM KCl, 1 mM $MgCl_2$, 5 mM HEPES, 1 mM $CaCl_2$, and 3 mM EGTA, with pH adjusted to 8.0 with KOH. The bath compartment was connected via a 3-M agar bridge to a ground compartment containing the same solution. After excision of patches containing single hemichannels, instrumentation offsets were manually corrected in the absence of an applied voltage. Single hemichannel I-V curves were obtained by applying 8-s voltage ramps from −70 to 70 mV. Currents were leak subtracted by measuring leak conductance of a given patch from full closing transitions and extrapolating linearly over the entire voltage range. Because single hemichannel currents were not linear with voltage, conductance was measured as the slope conductance obtained from linear fits of leak-subtracted currents of ∼0 mV. In experiments examining the accessibility of methanethiosulfonate (MTS) reagents, excised patches were maintained at a fixed voltage to which MTS reagents were applied by addition to the bath. Bath volume was ∼0.3–0.4 ml. Single hemichannel I-V curves were obtained before and after MTS application by applying 8-s voltage ramps from −70 to 70 mV.

For measurements of junctional conductance (g_j) in *Xenopus* oocytes, cells were manually devitellinized and paired by placing in dishes coated with 1% agarose. Each oocyte of a pair was clamped independently using a two-electrode voltage clamp to a common potential (typically −40 mV). V_j steps, 10 s in duration, were applied by stepping the voltage in one cell of a pair over a range of ±120 mV in 10-mV increments; the voltage in the other cell remained constant. Each V_j step was preceded by a small, brief prepulse of constant amplitude (10 mV) so that a family of currents could be normalized if the expression level changed over the course of an experiment. The cells were allowed to recover for 90 s between V_j steps. Currents were filtered at 200 Hz and digitized at 1–2 kHz. Steady-state currents were obtained by extrapolating exponential fits of the data to $t = \infty$ as previously described (Verselis et al., 1994). Only cell pairs with g_j values ≤5 µS were used to avoid effects of series access resistance on voltage dependence (Wilders and Jongsma, 1992).

In mammalian N2A cells, electrophysiological measurements were performed using the dual whole-cell patch clamp method at room temperature as previously described (Meşe et al., 2008). At the beginning of each experiment, both cells were clamped at the same holding potential. Then, one of the cells was stepped to different voltages (±10–110 mV in 20-mV increments). The current from the cell held at constant potential was recorded and divided by the voltage to calculate conductance.

In all electrophysiological recordings, data were acquired with AT-MIO-16X D/A boards (National Instruments) using custom acquisition software (written by E.B. Trexler, Mt. Sinai School of Medicine, New York, NY). In patch clamp experiments, currents were typically filtered at 1 kHz, and data were acquired at 5 kHz.

Preparation of MTS reagents

2-trimethylammonioethyl-methanethiosulfonate (MTSET) and sodium (2-sulfonatoethyl) methanethiosulfonate (MTSES) were purchased from Anatrace. Aliquots of dry powder were prepared and stored in microcentrifuge tubes at −20°C. Before each experiment, aliquots of MTSET and MTSES were dissolved in distilled water and chilled on ice to stock concentrations of 250 mM. Dilutions were made into appropriate perfusion solutions just before application to a final concentration of 0.2 mM for MTSET and 2 mM for MTSES. Activity of MTS reagents were periodically checked using the 5-thio-2-nitrobenzoate assay (Karlin and Akabas, 1998).

RESULTS

Hemichannels containing the A40V mutation have impaired regulation by Ca^{2+}

Fig. 1 (A–C) shows families of normalized conductance-voltage (G-V) relationships of WT Cx26, G45E, and A40V mutant hemichannels. In each of the representative examples shown, a family of G-V curves was obtained from a single oocyte exposed to successive changes in extracellular Ca^{2+} concentration ranging from 0 (nominal) to 2.0 mM. Lowering extracellular Ca^{2+} potentiated currents of WT Cx26 as well as A40V and G45E mutant hemichannels and strongly shifted their G-V relations in a hyperpolarizing direction. G45E and A40V differed from WT Cx26, particularly A40V, which showed little change in conductance between 0 (nominal) and 0.2 mM of added Ca^{2+}. G45E hemichannels also showed a weaker response in this range of Ca^{2+}. At physiological Ca^{2+} concentrations, in the 1.0–2.0-mM range, WT and mutant hemichannels showed currents distinctly above baseline even when the membrane potentials were modestly negative (i.e., in the −40 to −50–mV range). However, all the hemichannels could be effectively closed with stronger hyperpolarization and activated robustly when the membrane potential was depolarized to positive values. In addition, G45E showed altered voltage dependence at positive membrane potentials, with conductance declining at voltages exceeding 30 mV.

Because voltage dependence of Cx26 hemichannels exhibits slow kinetics (González et al., 2006; Gerido et al., 2007), we sought to obtain steady-state Ca^{2+} response curves by perfusing simple salt solutions (100 mM NaCl) containing various Ca^{2+} concentrations while maintaining the oocytes at a fixed holding potential of −40 mV, a membrane potential that is close to that of human keratinocytes (Wohlrab et al., 2000). Examples of recordings of hemichannel currents are shown for oocytes expressing WT Cx26 and A40V (Fig. 2 A). In both cases, exposure to a solution with 0 added (nominal) Ca^{2+} caused robust opening evident by the development of a large inward current. Successive exposures to solutions containing increasing concentrations of Ca^{2+} showed progressive reductions in current for WT Cx26 hemichannels. A40V hemichannels, however, showed little change until the Ca^{2+} concentration exceeded 0.3 mM. Ca^{2+} response curves for all three hemichannel types compiled from several experiments are summarized in Fig. 2 B.

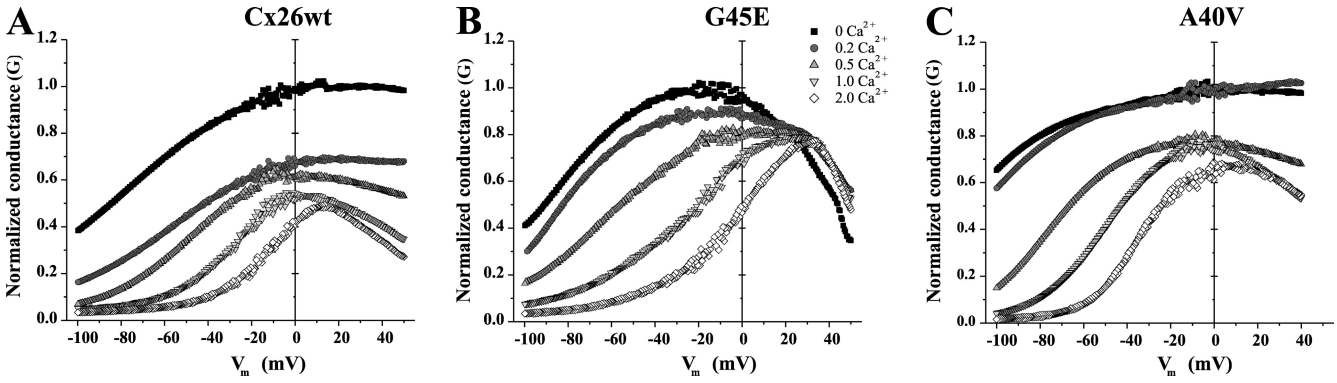

Figure 1. Regulation of WT Cx26 and A40V and G45E mutant hemichannels by voltage and extracellular Ca^{2+}. Representative conductance-voltage (G-V) relationships are shown expressed in *Xenopus* oocytes at different external Ca^{2+} concentrations ranging from nominal (0 added) to 2 mM obtained by applying slow (3 min) voltage ramps from 50 to −100 mV to oocytes expressing WT Cx26 (A), G45E (B), or A40V (C). The holding potential before and after each ramp was maintained at −20 mV. All conductances were normalized to the maximum value measured in 0 Ca^{2+}. In WT and both mutant hemichannels, conductance declined strongly with hyperpolarization except in low extracellular Ca^{2+}. Increasing Ca^{2+} shifted activation in the depolarizing direction in all cases. However, both mutant hemichannels appeared less sensitive to the effects of Ca^{2+}, particularly at low Ca^{2+} concentrations. This reduced sensitivity to Ca^{2+} was strongest in A40V. In addition, G45E hemichannels showed stronger voltage-dependent closure at positive voltages (up to 50 mV).

For A40V, the steady-state response to Ca^{2+} is shifted substantially rightward, and a considerable steady-state current remained even when the Ca^{2+} concentration was in the 1–2-mM range. The steady-state Ca^{2+} response of G45E is somewhat shifted compared with WT Cx26, but only at lower Ca^{2+} concentrations; there is little difference between Cx26 and G45E at concentrations ≥1 mM.

To assess the impact of having WT and mutant Cx26 hemichannels expressed in oocytes bathed in a fixed Ca^{2+} concentration over a longer time period, we measured the resting potentials of cells left undisturbed in ND96 containing 1.8 mM Ca^{2+}. The potentials were measured in a 24–48-h window after injection, before any visible signs of cell death, such as membrane blebbing and altered pigmentation. Cells injected with WT Cx26 and

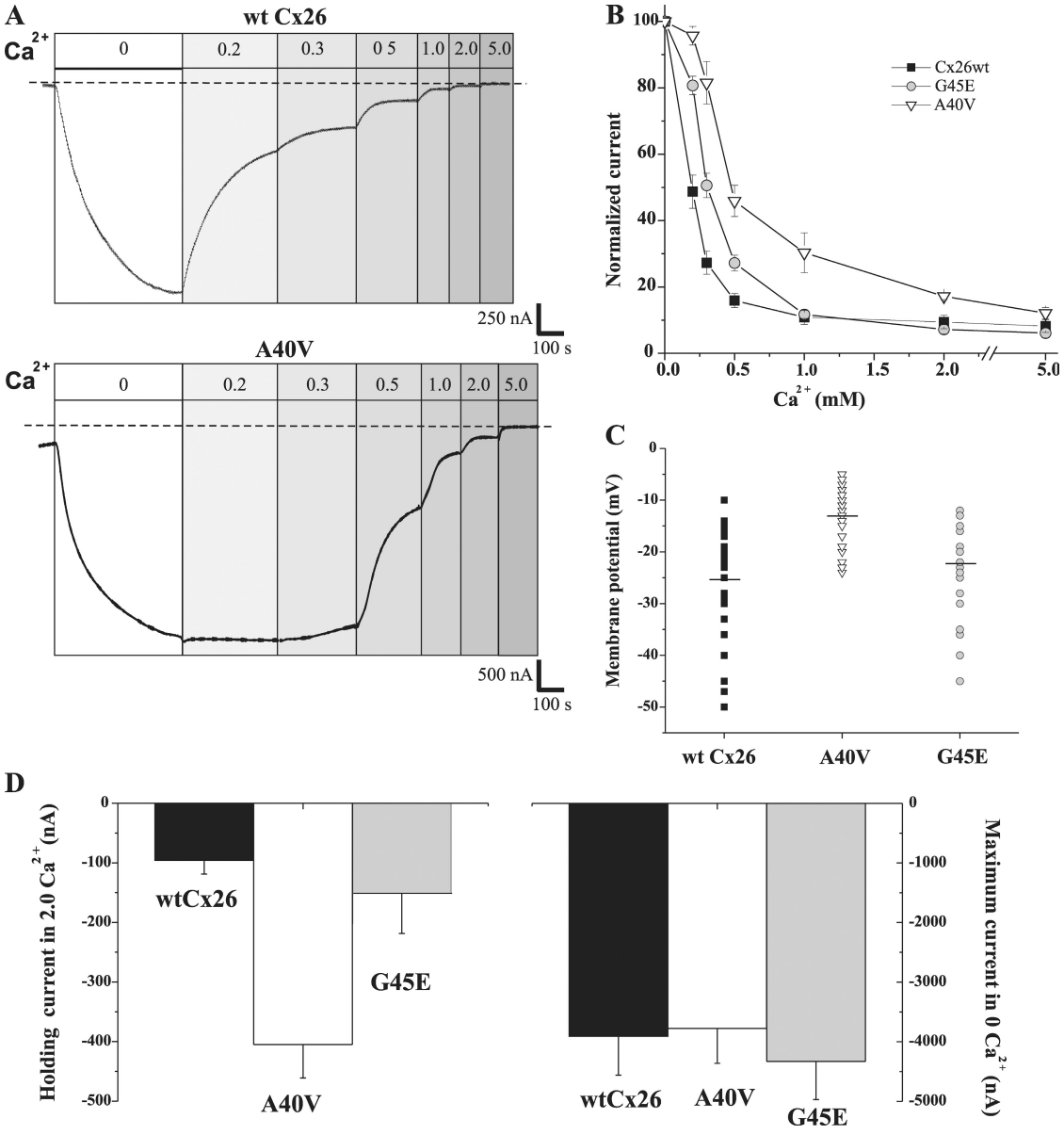

Figure 2. Steady-state Ca^{2+} response curves show that A40V hemichannels are less sensitive to external Ca^{2+} than WT Cx26 and G45E hemichannels. (A) Examples of recordings of WT Cx26 (top) and A40V (bottom) hemichannel currents and effects of increasing concentrations of extracellular Ca^{2+} (0, 0.2, 0.3, 0.5, 1.0, 2.0, and 5.0 mM). Oocytes were voltage clamped and maintained at −40 mV throughout. (B) Summary of data for WT Cx26 (■), A40V (∇), and G45E (○) compiled from several experiments such as that shown in A. Each point is the mean ± SEM of ∼20 experiments. (C) Plot showing resting membrane potentials measured in oocytes 24–48 h after RNA injection for WT Cx26 (■), A40V (∇), and G45E (○). Each point represents a measurement from an individual oocyte. Horizontal lines represent means of −25.1 ± 9.4 mV, −13.1 ± 5.5 mV, and −22.3 ± 8.0 mV for WT Cx26, A40V, and G45E, respectively. (D) The left panel shows the mean holding currents for oocytes from C when initially clamped to −40 mV. A40V-expressing oocytes, which showed the lowest resting potentials, showed the largest holding currents. The same oocytes exposed to 0 added Ca^{2+} (right) showed similar maximum current levels, indicating similar levels of expression.

G45E exhibited a similar range of resting potentials, with means of −25.1 mV and −22.3 mV, respectively (Fig. 2 C). However, the cells injected with A40V were substantially depolarized with a mean potential of −13.1 mV. These lower resting potentials in A40V were accompanied by larger holding currents upon voltage clamping to −40 mV (Fig. 2 D, left), which could be reversibly reduced by elevating extracellular Ca^{2+} (not depicted), indicating it was mediated by hemichannels and not by generally compromised membrane integrity. Exposure of the cells to a solution containing 0 added (nominal) Ca^{2+} resulted in a similar range of maximum current

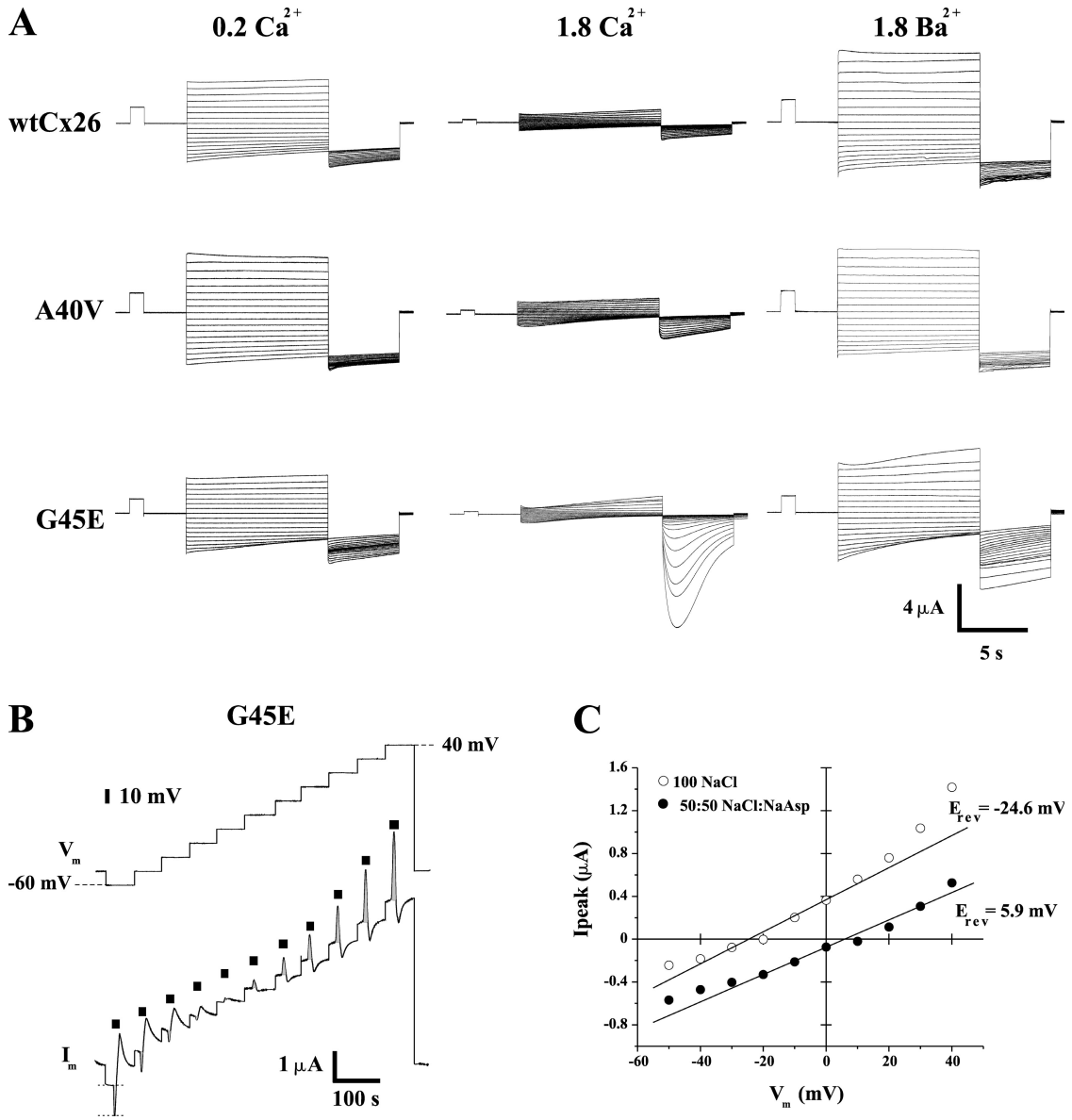

Figure 3. G45E hemichannels exhibit increased permeability to Ca^{2+}. (A) Representative currents elicited by a series of voltage steps applied to oocytes expressing WT Cx26, A40V, and G45E. Oocytes were voltage clamped to −20 mV. The applied voltage step protocol consisted of 10-s steps from 60 to −100 mV in intervals of 10 mV followed by a 5-s step to −110 mV. Each series was repeated in extracellular solutions containing 0.2 mM Ca^{2+}, 1.8 mM Ca^{2+}, and 1.8 mM Ba^{2+}. Currents from oocytes expressing any one of the three hemichannel types were similar in low Ca^{2+} (0.2 mM). Upon raising Ca^{2+} to 1.8 mM, a large transient inward current developed in oocytes expressing G45E when the voltage was stepped to −110 mV after depolarizing steps that activated these hemichannels. Equimolar substitution of Ca^{2+} with Ba^{2+} abolished the large transient inward current. Also, the hemichannel currents in Ba^{2+} resembled those in low Ca^{2+}. (B and C) The transient current observed in oocytes expressing G45E represents a Ca^{2+}-activated chloride current. (B) A representative recording of the reversal potential of the transient current for an oocyte bathed in 100 mM NaCl and 0.2 mM Ca^{2+}. At various voltages (as indicated), oocytes were briefly exposed to 1.8 mM Ca^{2+} (indicated by the black boxes). The transient current that developed (filled in gray) reversed between −20 and −30 mV and was followed by a decay in the hemichannel current that reversed upon returning to 0.2 mM Ca^{2+}. This protocol was repeated in an external solution in which 100 mM NaCl was replaced with a 50:50 NaCl/NaAsp. (C) Plot of peak transient current after exposure to 1.8 mM Ca^{2+} in 100 mM NaCl and 50:50 NaCl/NaAsp. Reversal potential shifted in accordance with the change in the extracellular Cl concentration.

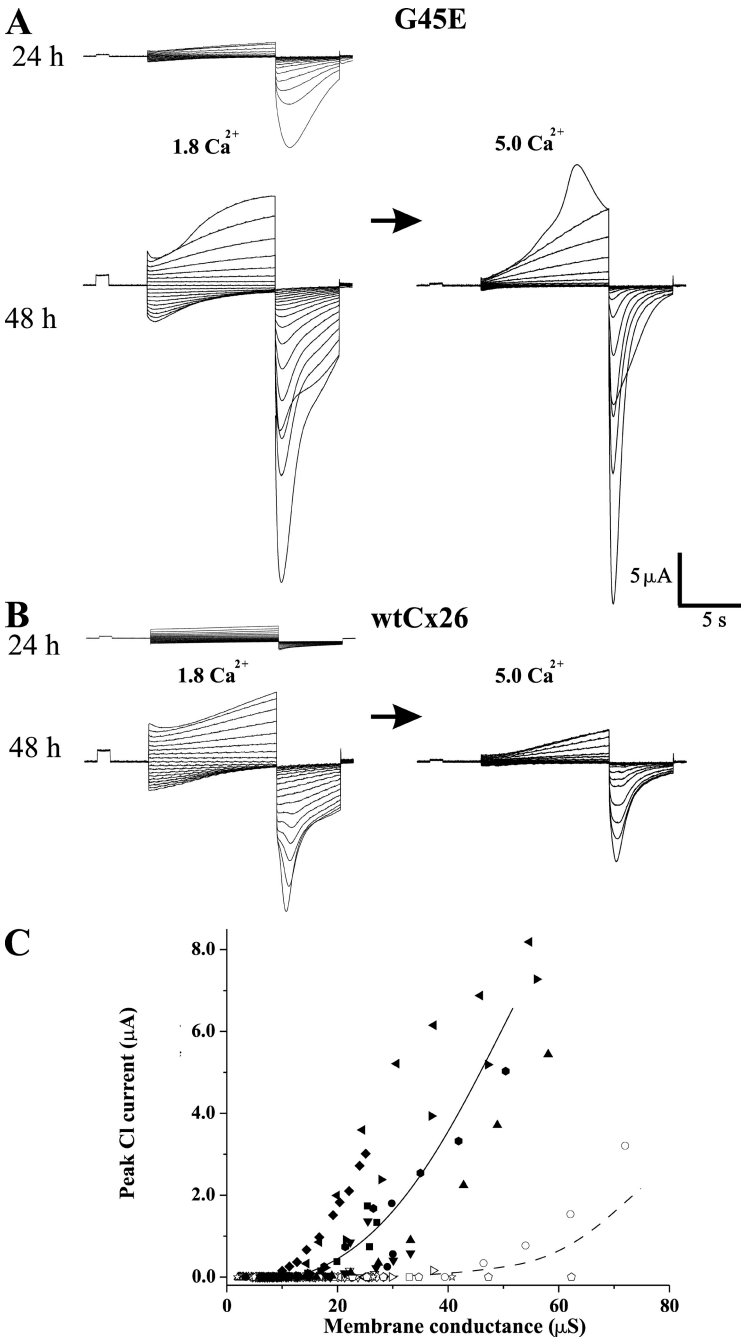

Figure 4. WT Cx26 hemichannels are also permeable to Ca^{2+}. (A and B) Currents from oocytes expressing G45E (A) and WT Cx26 (B) recorded 24 and 48 h after injection of RNA. At 48 h, recordings are shown in 1.8 and 5.0 mM extracellular Ca^{2+}. Voltage step protocols are the same as in Fig. 3 A. At 48 h, oocytes expressing G45E show larger hemichannel currents in 1.8 Ca^{2+} (compared with 24 h) along with larger Ca^{2+}-activated Cl currents. Upon raising Ca^{2+} to 5 mM, G45E hemichannels continued to activate at positive voltages and to induce Ca^{2+}-activated Cl currents. With increased expression of WT Cx26 hemichannels, Ca^{2+}-activated Cl currents were also induced, albeit more weakly in comparison to G45E. (C) Peak chloride current is plotted as a function of the membrane conductance. Measurements were obtained from the same voltage protocol as shown in A and B). The magnitude of the chloride current was measured at the peak that developed at −110 mV after the activating voltages steps. Baseline was taken as the instantaneous current upon stepping to −110 mV that preceded the development of the large inward transient. The membrane conductance was measured at the end of the activating voltage step, the bulk of which was caused by hemichannel activation. Open symbols are data from WT Cx26, and closed symbols are from G45E. Experiments from individual oocytes are plotted as different symbol shapes. Lines represent fits (by eye) to the data for illustration purposes. n = 8 oocytes for G45E, and n = 9 oocytes for WT Cx26.

amplitudes in all three hemichannel types (Fig. 2 D, right), indicating that the effects were not caused by differences in hemichannel current levels. These data are consistent with A40V exhibiting a much greater degree of leaky hemichannel activity than G45E.

G45E hemichannels show increased Ca^{2+} permeability

When we examined currents from WT Cx26, A40V, and G45E hemichannels in response to their activation by depolarizing voltage steps, we observed that opening of G45E hemichannels led to robust activation of a Ca^{2+}-activated chloride current that is endogenous to *Xenopus* oocytes (Barish, 1983; Kuruma and Hartzell, 1999). Fig. 3 A shows WT Cx26 and mutant hemichannel currents in response to a series of activating voltage steps (10 s) ranging from 60 to −110 mV followed by a step to a common test voltage of −110 mV. In each case, the holding potential was −20 mV. Families of currents are shown in low (0.2 mM) and high (1.8 mM) Ca^{2+} conditions from oocytes exhibiting comparable hemichannel current amplitudes. In low (0.2 mM) Ca^{2+}, currents for all three hemichannels appear similar, showing weak voltage dependence over the tested range. Upon elevating Ca^{2+} to 1.8 mM, the currents in response to the activating voltage steps substantially decreased in magnitude at both positive and negative voltages as a

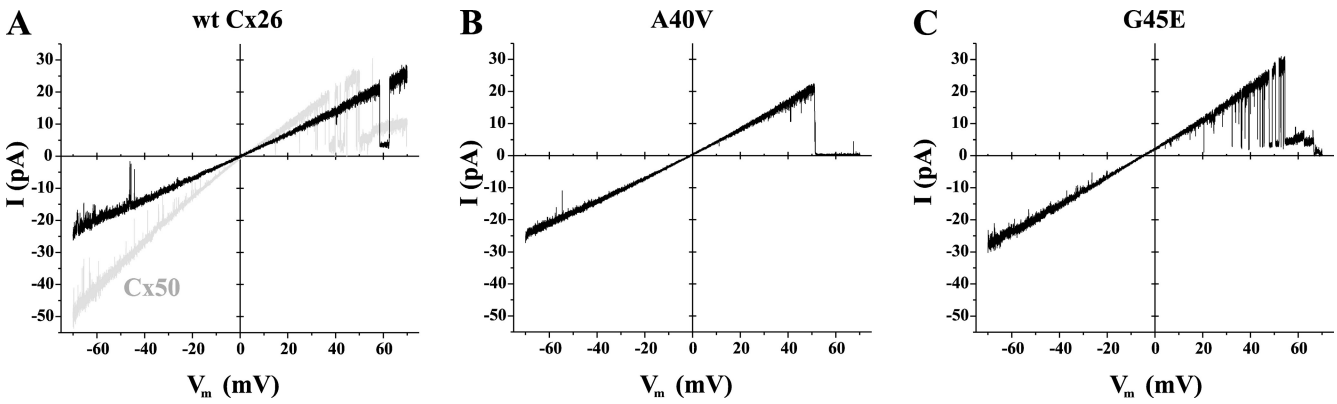

Figure 5. G45E hemichannels exhibit a larger unitary conductance. Representative examples of patch clamp recordings from inside-out patches containing single WT Cx26 (A), A40V (B), and G45E (C) hemichannels. The single hemichannel currents shown are in response to 8-s voltage ramps between ±70 mV and are leak subtracted (see Materials and methods). In contrast to other hemichannels that generally show inward current rectification in symmetric 140 mM KCl, WT Cx26 shows slight outward rectification. A recording of a single Cx50 hemichannel in the same solutions is included for comparison in A.

result of regulation by extracellular Ca^{2+}. However, after activation at positive voltages, hyperpolarization to the −110-mV test voltage elicited a large transient, inward current that peaked and decayed over a 5-s time course in oocytes expressing G45E but not WT Cx26 or A40V. Replacement of extracellular Ca^{2+} with Ba^{2+} abolished this large transient, inward current, indicating it was Ca^{2+} dependent. Furthermore, the reversal potential of the peak of the transient inward current followed the chloride reversal potential (Fig. 3, B and C). Collectively, these data indicate that the transient current is a Ca^{2+}-activated chloride current. The large magnitudes of the hemichannel currents in 1.8 mM Ba^{2+} indicate that Ba^{2+} is ineffective at regulating Cx26 hemichannels and does not activate chloride currents, at least at the concentrations we used.

When we examined oocytes with larger hemichannel currents, we observed a further increase in the magnitude of the Ca^{2+}-activated chloride current in G45E-expressing oocytes. Fig. 4 A shows G45E currents evaluated 24 and 36 h after injection of an oocyte that was kept at 16°C in the first 24 h and then at room temperature during the next 24–36-h interval. Currents on the left were obtained in ND96 containing 1.8 mM Ca^{2+}. Raising Ca^{2+} to 5 mM somewhat diminished the magnitude of the hemichannel current but provided a larger source of Ca^{2+} influx such that Ca^{2+}-activated chloride currents were occasionally activated on depolarization. Higher WT Cx26 hemichannel expression also was able to activate Ca^{2+}-activated chloride currents (Fig. 4 B), but typically activation was substantially weaker, even when the amplitudes of the hemichannel currents were comparable. This difference is illustrated in Fig. 4 C. A plot of the peak chloride current as a function of membrane conductance measured at the end of a series of activating pulses shows that oocytes expressing G45E exhibit Cl currents with less hemichannel activation compared with WT Cx26. In both cases, Cl currents positively correlate with the magnitude of the hemichannel conductance. Thus, WT Cx26 hemichannels are permeable to Ca^{2+}, but permeability is substantially increased in G45E hemichannels.

Single Cx26, A40V, and G45E hemichannels

Next, we sought to investigate how single G45E and A40V hemichannels compared with WT Cx26 hemichannels (Fig. 5). Recordings were obtained by patch-clamping oocytes, excising patches containing single hemichannels into symmetric 140-mM KCl solutions, and applying voltages ramps between −70 and 70 mV (8 s in duration). Currents of single open WT Cx26 hemichannels exhibited slight outward rectification over this voltage range and a mean slope conductance, measured at 0 mV, of 340 ± 9 pS (n = 7). An example of a recording of a single WT Cx26 hemichannel is shown in Fig. 5 A superimposed with a recording from a different connexin hemichannel, Cx50, which exhibits an ∼2:1 inward current rectification and a slope conductance of ∼470 pS in the same solutions. A40V hemichannels (Fig. 5 B) showed no significant difference in unitary conductance (mean slope conductance was ∼345 ± 19 pS, n = 10) or open hemichannel current rectification compared with WT Cx26. However, G45E hemichannels exhibited an ∼25% higher unitary conductance (∼435 ± 23 pS, n = 14; Fig. 5 C). Open hemichannel current remained slightly outward rectifying.

Cysteine substitution and accessibility studies: macroscopic currents

We individually introduced cysteines at A40 and G45 so that we could examine accessibility to thiol-modifying reagents. Cysteine substitution at each position resulted in functional hemichannels. G45C hemichannels differed, however, in that the addition of a heavy metal chelator, such as N,N,N′,N′-tetrakis(2-pyridylmethyl)ethylenediamine

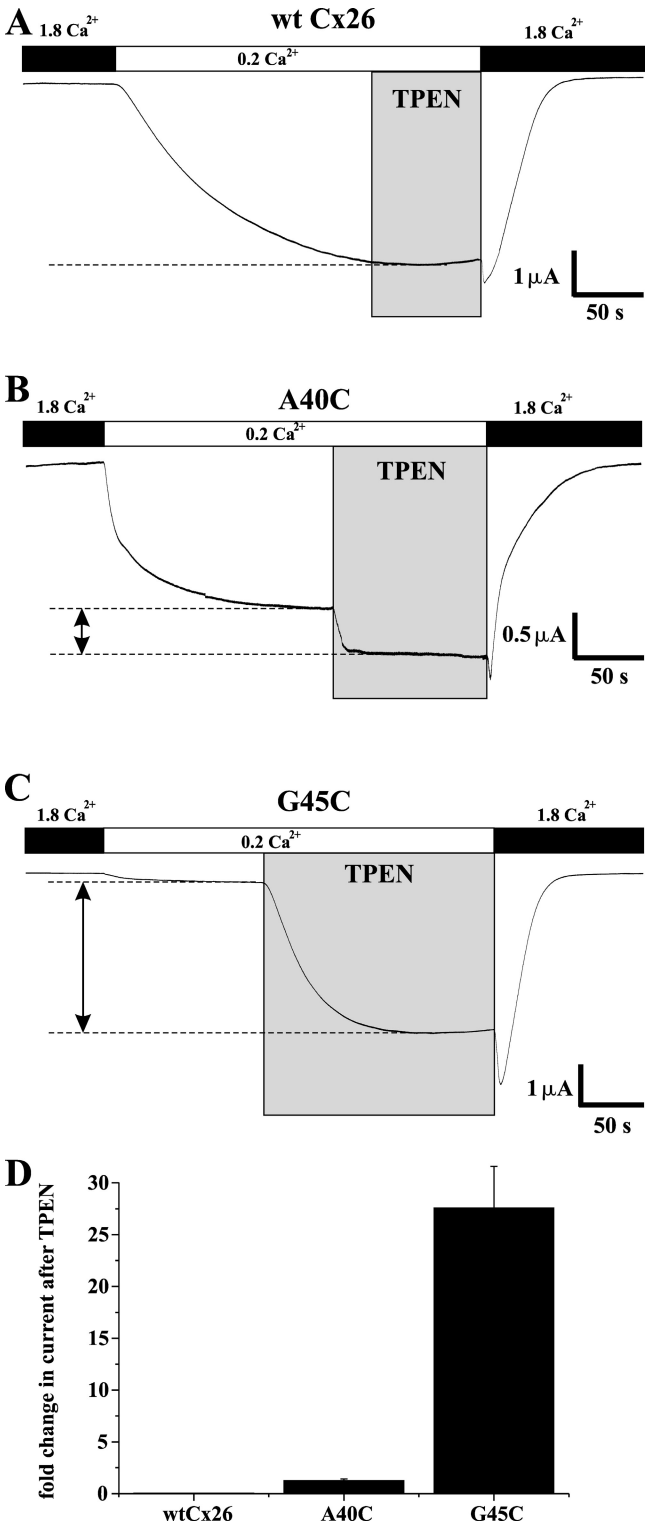

Figure 6. Cysteine substitutions at A40 and G45 produce functional hemichannels, but G45C exhibits impaired function as a result of coordination of metal ions. (A–C) Current traces from oocytes are shown expressing WT Cx26 (A), A40C (B), and G45C (C). Oocytes were held at −40 mV throughout and were exposed to a low extracellular Ca^{2+} (0.2 mM) solution with and without 10 μM of the heavy metal chelator TPEN. Oocytes expressing G45C show little current in 0.2 mM Ca^{2+} in the absence of TPEN and a large potentiation >10-fold after addition of TPEN. A40C hemichannel currents are robust in the absence of TPEN, and a small increase occurred after addition. TPEN had no effect on WT Cx26 hemichannels, which were robust upon lowering Ca^{2+} to 0.2 mM. (D) Summary of the effects of TPEN. Each bar represents the fold change (mean ± SEM) in current after TPEN in 0.2 mM Ca^{2+} ($n = 9$ for WT Cx26, $n = 17$ for A40C, and $n = 51$ for G45C).

(TPEN), substantially potentiated the magnitude of the current (Fig. 6 C). This property of G45C is similar to that reported for cysteine substitutions at the equivalent Gly residue in Cx50 and chimeric Cx32*43E1 hemichannels where the TPEN effect was ascribed to the formation of a high affinity metal-binding site involving the introduced cysteines (Tang et al., 2009; Verselis et al., 2009). In contrast, A40C currents were large in the absence of TPEN, but addition of TPEN did have a modest effect (Fig. 6 B). TPEN had no effect on WT Cx26 (Fig. 6 A). Data compiled from several experiments are summarized in Fig. 6 D.

Next, we examined the accessibility of G45C and A40C to MTS reagents by monitoring effects on macroscopic currents (Fig. 7). We used two MTS reagents, MTSET and MTSES, which upon modification would introduce side chains of opposite charge, positive and negative, respectively (Karlin and Akabas, 1998). For WT Cx26 hemichannels, neither reagent produced an effect (recording not depicted). However, application of MTS reagents to oocytes expressing G45C hemichannels produced robust effects that differed for the two reagents. MTSET produced a large, rapid decrease in current of ∼70% (Fig. 7 A, left), whereas MTSES caused a rapid increase of ∼30% (Fig. 7 A, right). For A40C hemichannel currents, application of these MTS reagents also produced effects, but for both reagents the effects consisted of reductions in current of ∼30–40% that were considerably slower in time course (Fig. 7 B). Data compiled from several experiments are summarized in Fig. 7 C.

SCAM applied to single hemichannels

To determine if G45C and A40C reside in the aqueous pore, we excised patches containing single hemichannels and exposed them to either MTSET or MTSES added to the bath. Both inside-out and outside-out patches were used to examine accessibility from extracellular and intracellular sides of the hemichannel, with the expectation that residues in the pore would be accessible from either side of an open hemichannel and that the effects would manifest as changes in open hemichannel properties. Moreover, the changes in open hemichannel properties should differ between the two reagents because of the introduction of oppositely charged side changes into the ion permeation pathway.

At the single-channel level, G45C hemichannels were similar to WT Cx26 hemichannels, displaying slight outward current rectification of the open state and a unitary

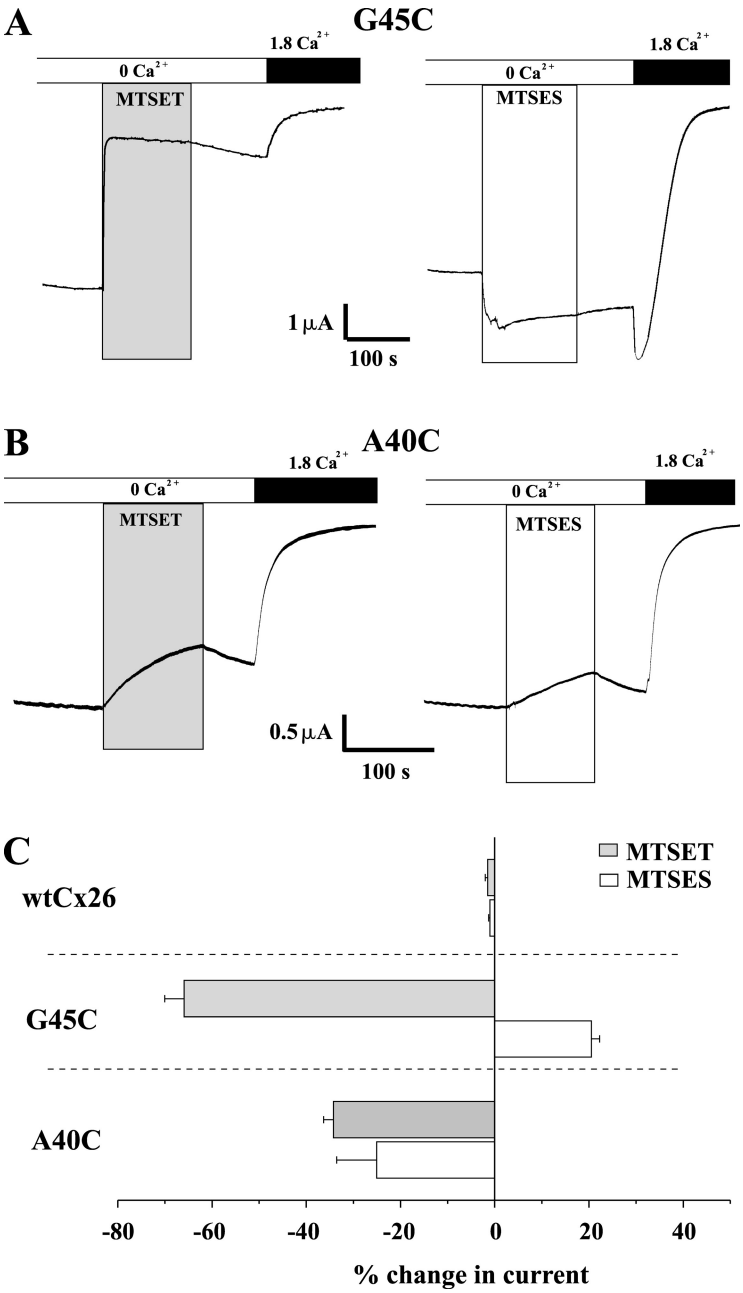

Figure 7. SCAM experiments using different MTS reagents show robust and differential effects on G45C. (A and B) The effects of MTS reagents on hemichannel currents are shown from G45C (A) and A40C (B) recorded at −40 mV. Before the recordings shown, oocytes were exposed to a solution containing 3 mM EGTA (0 Ca^{2+}) to open hemichannels and then were exposed to the same solution containing 0.2 mM MTSET (positively charged, left) or 2.0 mM MTSES (negatively charged, right). G45C currents showed rapid and robust response to both MTS reagents that were opposite in sign, decreasing for MTSET and increasing for MTSES. Both MTS reagents decreased A40C currents, but the effects were more modest and slow in time course. (C) Summary of the percent change in current (mean ± SEM) upon application of the MTS reagent. n = 5 for WT Cx26, n = 7 for A40C, and n = 24 for G45C for MTSET. n = 7 for WT Cx26, n = 7 for A40C, and n = 23 for G45C for MTSES.

conductance of ∼353 ± 20 pS (n = 19) measured as the slope conductance at V_m = 0 in 140 mM KCl (Fig. 8 B, left). Application of MTSET to a single G45C hemichannel in an excised patch maintained at a constant potential led to a stepwise reduction in unitary current to a final level that was ∼70% reduced in amplitude (Fig. 8 A, top trace). Conversely, application of MTSES led to a stepwise increase in unitary current of ∼30% (Fig. 8 A, bottom trace). Thus, changes in the magnitude of the unitary current largely underlie the effects observed in the macroscopic recordings. Open hemichannel currents in response to ±70-mV voltage ramps are shown before and after MTS application (Fig. 8 B). The large reduction in unitary conductance with MTSET accompanied a loss of the slight outward rectification characteristic of the unmodified G45C hemichannel over a ±70-mV range. MTSES-modified G45C hemichannels continued to show modest outward rectification. The same changes in open hemichannel properties occurred when reagent was applied from the cytoplasmic or extracellular sides. Thus, the MTS effects observed macroscopically for G45C are consistent with a location in the aqueous pore.

A40C hemichannels had a somewhat smaller conductance of 310 ± 21 pS (n = 7) than WT Cx26 hemichannels (Fig. 8 C, left). Also, these hemichannels tended to spend longer times in a fully closed state compared with WT Cx26 and G45C hemichannels. However, we saw no significant change in unitary conductance upon

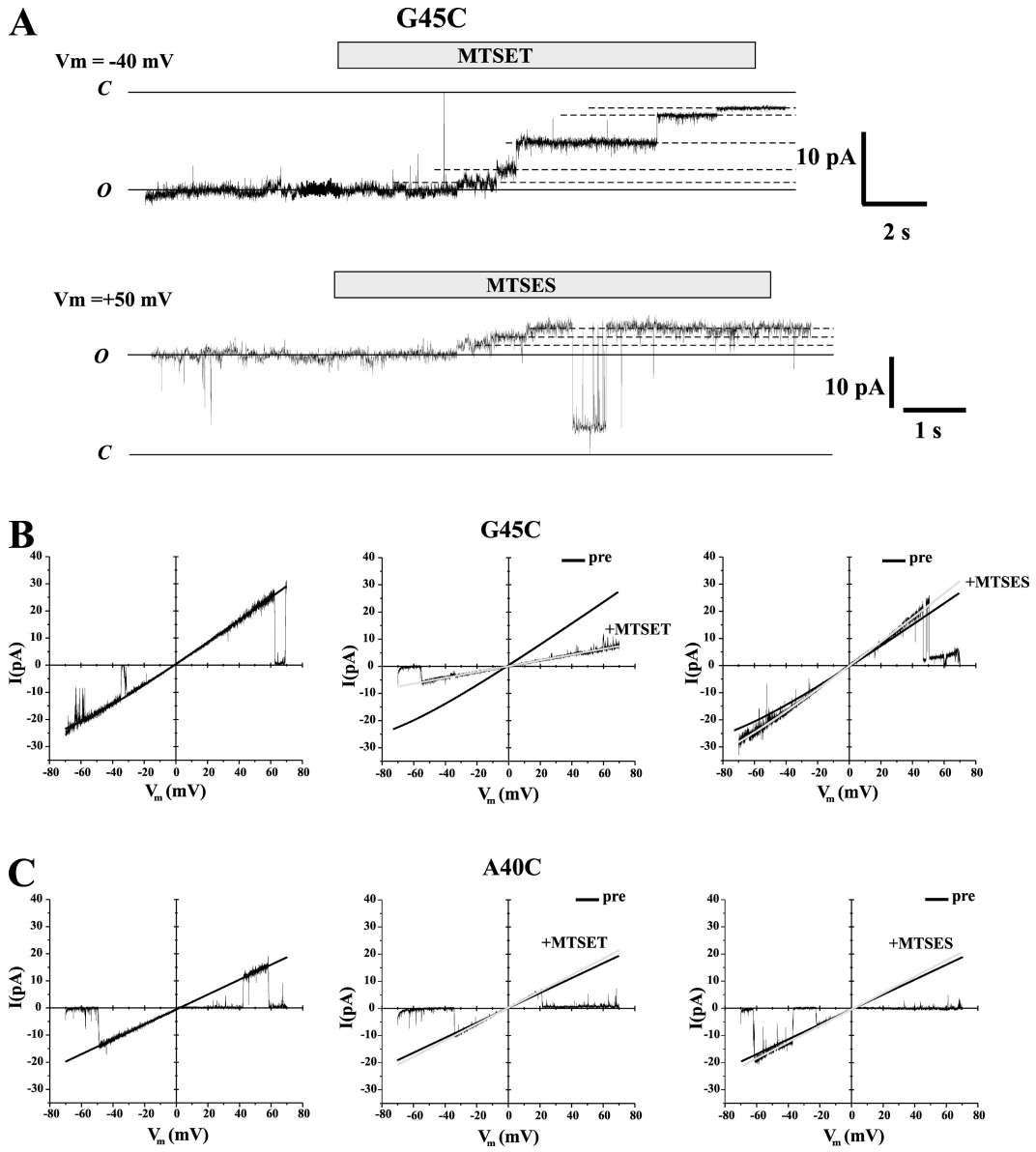

Figure 8. Single-channel SCAM indicates that G45 is a pore-lining residue. (A) Recordings of single G45C hemichannels in excised patches. The top trace is a recording from an inside-out patch held at −40 mV. Exposure to MTSET produced a stepwise reduction in current (discernable levels indicated by dashed lines). The bottom recording is from an outside-out patch held at 40 mV. Exposure to MTSES produced a stepwise increase in current (discernable levels indicated by dashed lines). *C* and *O* depict fully closed and open states in both traces. (B) Examples of G45C hemichannel currents before and after (3 min) application of MTS reagents. The left panel shows a single G45C hemichannel recording in the absence of added reagent. The solid line is a fit to the open hemichannel current. The middle and right panels show effects of MTS reagents. Solid black lines represent fits to the open hemichannel I-V relationships before MTS application. Data and fits (gray lines) are after MTS application. (C) Same as in B for single A40C hemichannels. All currents were elicited by 8-s voltage ramps between ±70 mV. Currents were leak subtracted as described in Materials and methods.

application of either MTS reagent. There appeared to be a tendency to spend more in the closed state after exposure to MTS reagents, but this was not quantified. Open A40C hemichannel currents before and after application are shown in Fig. 8 C. We could not adequately test reactivity from the cytoplasmic side because the A40C hemichannel tended to be unstable upon excision in an inside-out configuration. Nonetheless, the lack of an effect on open hemichannel conductance, together with the similarities of the effects of MTSET and MTSES, is not consistent with A40C being a pore-lining residue. It is likely that the effects of MTS reagents on A40C observed macroscpoically are related to changes in gating and/or Ca^{2+} regulation, but we did not explore this further.

G45E and A40V cell–cell channels

Although both G45E and A40V have been shown to function as hemichannels, only G45E was reported to

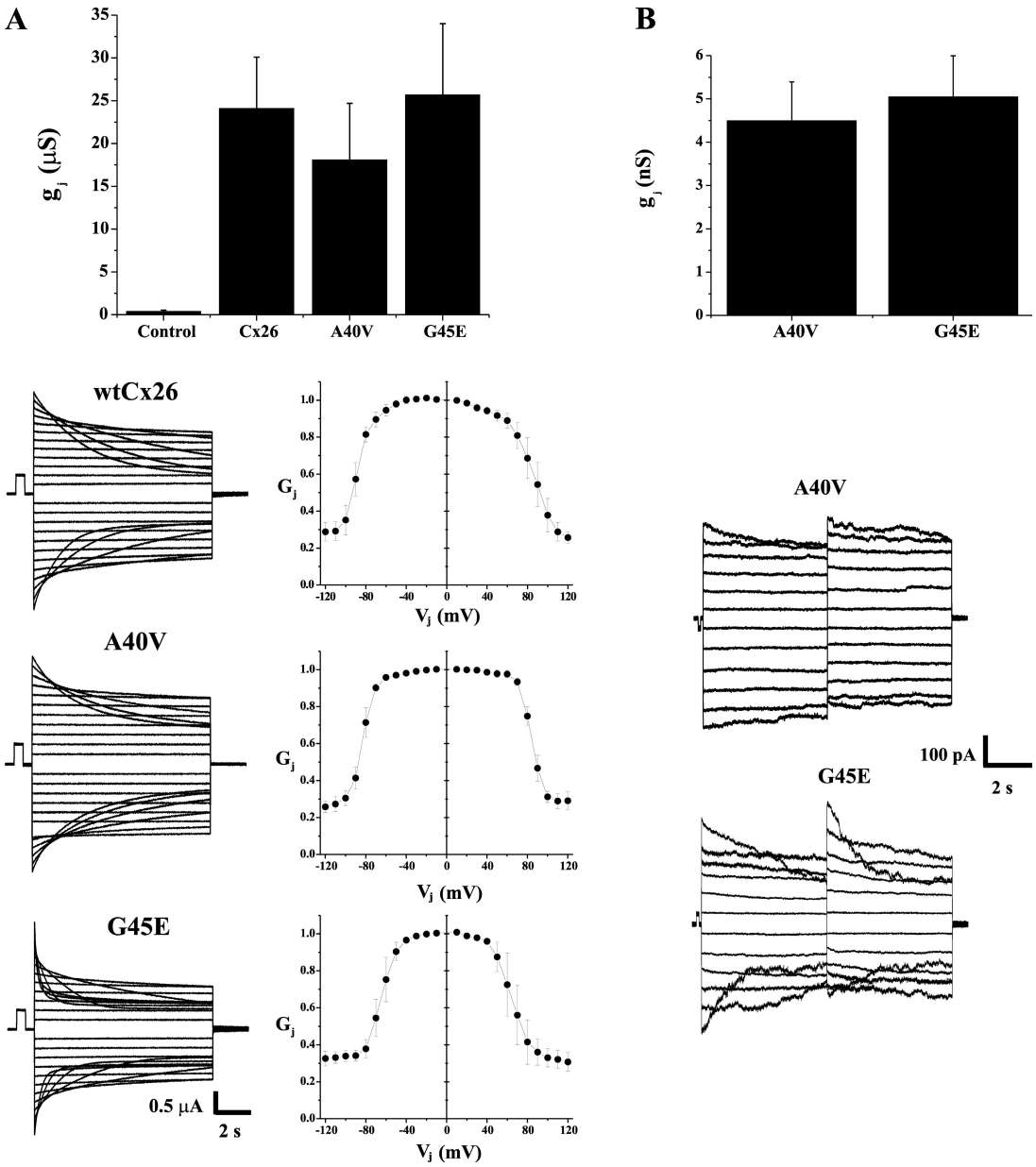

Figure 9. A40V and G45E mutants make functional cell–cell channels. (A) Bar graph showing junctional conductances, g_j (mean ± SEM), measured in oocyte pairs injected with H_2O (control, $n = 10$), WT Cx26 ($n = 12$), A40V ($n = 8$), and G45E ($n = 7$). Coupling was robust for WT Cx26 and both mutants compared with the control. Representative examples of junctional currents (left) along with steady-state G_j-V_j relationships (right) obtained from WT Cx26 ($n = 4$), A40V ($n = 3$), and G45E ($n = 4$) cell pairs. G_j is g_j normalized to the maximum about $V_j = 0$. Records were taken from oocytes that were paired for shorter times to avoid series access resistance errors that accompany strong coupling. V_j steps between ±120 mV were applied in 10-mV increments. (B) Bar graph showing junctional conductances (mean ± SEM) measured in N2A cell pairs transfected with A40V and G45E ($n = 42$ for A40V, and $n = 53$ for G45E). Examples of junctional currents are shown below. V_j steps between ±120 mV were applied in 10-mV increments.

function as a cell–cell channel using the paired oocyte expression system (Gerido et al., 2007). The assessment of A40V to function as a cell–cell channel was made difficult by the fact that the oocytes tended to die rapidly when expressing this mutant. Thus, we paired oocytes and incubated them at cooler temperatures (10°C) to reduce that rate of A40V expression but allow time for cells to adhere and initiate junction formation. In other cells, we decreased the volume of RNA injected and paired A40V oocytes in parallel with G45E and WT Cx26 at similar dilutions. Expression in all cases was evaluated by measuring the magnitude of the hemichannel current. Regardless of the procedure used, A40V cell pairs showed strong coupling, similar to WT Cx26 and G45E cell pairs (Fig. 9 A). Conductance-voltage relations and examples of corresponding junctional currents are shown for each hemichannel type. Voltage dependence of A40V was very similar to WT Cx26, whereas G45E was

more sensitive to voltage as previously reported (Gerido et al., 2007).

We also transfected N2A cells with A40V and G45E and examined coupling in cell pairs using the dual whole-cell patch clamp configuration. As in oocytes, both mutants induced good coupling in N2A cell pairs (Fig. 9 B). Also, the voltage dependence of G45E was more pronounced than that of A40V, which is consistent with the data obtained from *Xenopus* oocyte cell pairs.

DISCUSSION

In this paper, we examined two missense mutations in Cx26, A40V, and G45E, that are associated with KID syndrome. Individuals with KID syndrome display overlapping phenotypes consisting mainly of sensorineural hearing loss, ichthyosis, hyperkeratosis, and keratitis with progressive corneal opacification that results in visual impairment. Often, there is increased susceptibility to mucocutaneous infection, and in the case of G45E, this has proven fatal as a result of uncontrollable sepsis (Janecke et al., 2005). Both mutations have been reported to produce hemichannels with altered properties characterized as dysregulated or leaky that result in compromised cell integrity and cell death (Stong et al., 2006; Gerido et al., 2007). Because connexin channels, in general, are large and poorly selective among monovalent inorganic ions (Verselis and Veenstra, 2000; Harris, 2001; Goldberg et al., 2004), increased hemichannel activity will not only promote leakage/entry of signaling molecules and metabolites but will also tend to drive the membrane potential toward 0 mV.

We found that A40V did exhibit a substantially altered sensitivity to extracellular Ca^{2+}, increasing the likelihood that hemichannels open even when extracellular Ca^{2+} resides in the 1.0–2.0-mM range. We quantified this altered sensitivity at a fixed potential of −40 mV (Fig. 2 B), but the conductance voltage G-V relations in various Ca^{2+} concentrations (Fig. 1, A–C) suggest that this weakened sensitivity extends over a large voltage range. When oocytes injected with A40V were left undisturbed in 1.8 mM Ca^{2+}, there was sufficient hemichannel activity to run down the resting potentials over a 24–36-h period in comparison to oocytes injected with WT Cx26. Maximum current levels in the absence of added Ca^{2+} were similar in both, indicating that there were comparable numbers of functional WT and mutant hemichannels in the membrane. Thus, the characteristics of A40V are consistent with a leaky hemichannel phenotype. However, sufficiently large hyperpolarized potentials, beyond −70 mV, can effectively close A40V hemichannels. Thus, the effects of this mutation may differ in the cochlea as compared with skin. Deiter's support cells in the cochlea, which express Cx26, have a host of K^+ channels that have a strong hyperpolarizing influence and maintain a robust membrane potential in the range of −75 to −80 mV (Oesterle and Dallos, 1990; Lang et al., 2007), whereas keratinocytes, which also express Cx26, typically have a resting membrane potential in the −20 to −30–mV range (Wohlrab et al., 2000).

In contrast to A40V, we found that Ca^{2+} regulation of G45E hemichannels was only modestly impaired but that permeability to Ca^{2+} was enhanced. The preservation of Ca^{2+} regulation is consistent with the results of Gerido et al. (2007), who showed that oocytes bathed in the absence of added Ca^{2+} underwent rapid cell death within 12–24 h after injection, whereas those bathed in ≥2 mM Ca^{2+} maintained cell viability. Thus, high extracellular Ca^{2+} can protect G45E-expressing cells, at least transiently, by closing hemichannels even though their Ca^{2+} permeability is enhanced. Indeed, we observed that oocytes expressing G45E left undisturbed for 24–36 h did not run down their membrane potentials like those expressing A40V. Of note, we find that WT Cx26 is Ca^{2+} permeable, and the hemichannels may mediate Ca^{2+} signaling in normal tissue function. Thus, over a longer period of time, cells expressing G45E, with enhanced Ca^{2+} permeability and modest Ca^{2+} dysregulation, would likely tend toward increased intracellular Ca^{2+} levels and membrane depolarization, which could lead to a spiraling effect by opening more hemichannels and promoting more depolarization and Ca^{2+} entry. Like A40V, the effects of G45E will depend on the interplay between Ca^{2+} and voltage. Cells that have lower resting potentials or depolarize in response to physiological stimuli would likely be affected to a greater extent. Also, for some connexins, a rise in intracellular Ca^{2+} has been shown to promote further hemichannel activity (De Vuyst et al., 2006; Schalper et al., 2008; Sánchez et al., 2009). During the review of this manuscript, expression of two KID mutants, D50N and G11E, were reported to cause apoptotic and necrotic cell death in human keratinocytes that was associated with increased intracellular Ca^{2+} levels as a result of aberrant hemichannel opening (Terrinoni et al., 2010b).

Stong et al. (2006) observed a more robust weakening of Ca^{2+} regulation for G45E expressed in human embryonic kidney cells using a dye uptake assay. Because of their small size, human embryonic kidney cells are likely to be strongly depolarized even by modest hemichannel activity, and it is possible that Ca^{2+} regulation weakens at more depolarized potentials. Gerido et al. (2007) also observed another difference between G45E and WT Cx26 in that larger currents were observed for G45E at similar levels of protein expressed in the membrane. We generally did not observe larger currents for G45E compared with WT Cx26 but maintained oocytes at 16°C before recording and did not routinely measure RNA concentrations or protein levels. Our data indicate that differences in unitary conductance and gating in the absence of Ca^{2+} cannot account for such a difference in current levels. Thus, it is possible that the G45E mutation imparts increased functional

efficiency compared with WT Cx26, but this property may be specific to cell type and experimental conditions.

Mutations that cause syndromic deafness cluster in NT and E1, principal pore-forming and gating domains

Over 100 mutations in Cx26 have been associated with nonsyndromic deafness (Lee et al., 2009). Many of these mutations are autosomal recessive and represent loss-of-function as a result of frameshifts and severe truncations of the Cx26 protein. Mutations that cause syndromic deafness associated with skin disorders are less common and constitute missense mutations that result in substitution of a single amino acid. These mutations are autosomal dominant and, interestingly, cluster in the NT and E1 domains.

The NT and E1 domains, along with TM1, play a central role in governing connexin channel permeability. Using SCAM studies in single Cx46 hemichannels, a stretch of amino acids starting midway through TM1 and extending into E1 was assigned to the pore (Zhou et al., 1997; Kronengold et al., 2003a, b). Although there has been controversy regarding the identities of the principal connexin pore-lining segments (for review see Verselis, 2009), a recent crystal structure of a Cx26 gap junction channel at 3.5-Å resolution (Maeda et al., 2009) shows agreement with the assignment of TM1 and E1 as well as NT; the latter forms that cytoplasmic vestibule of the pore in agreement with biophysical studies of Cx32 and Cx26 cell–cell channels (Verselis et al., 1994; Oh et al., 1999; Purnick et al., 2000b).

The G45E mutation, which is near the TM1/E1 border, occurs at a position that is predicted to be in the pore of Cx26 based on the crystal structure, and we demonstrate this to be the case using SCAM. Reactions with MTSES and MTSET increased and decreased unitary conductance, respectively. Cx26 exhibits a preference for cations (Suchyna et al., 1999; Meşe et al., 2008), and our results suggest that side chains that carry positive and negative charge at this position influence unitary conductance by decreasing and increasing cation flux, respectively. Accordingly, we observed that G45E hemichannels exhibited a larger unitary conductance and enhanced permeability to Ca^{2+}. Other positions predicted to be in the Cx26 pore that are linked to syndromic deafness include E42 and D50. Del42E has been linked to palmoplantar keratoderma (Richard, 2001), whereas D50N and D50Y have been linked to KID with additional clinical features of severe follicular occlusion triad and chronic mucocutaneous candidiasis, suggestive of immune system dysfunction (Richard et al., 2002; van Steensel et al., 2002; Yotsumoto et al., 2003; Janecke et al., 2005; Terrinoni et al., 2010a). Thus, several syndromic deafness mutants are likely pore mutations that may result in altered hemichannel permeability. D50N has been shown to form functional hemichannels when exogenously expressed in oocytes and adult human keratinocytes (Lee et al., 2009; Terrinoni et al., 2010b). Del42E has not been tested as a hemichannel, although it is known that Del42E fails to form gap junction channels (Rouan et al., 2001). The nature of the permeability change would presumably differ depending on the position and the nature of the substitution, thereby potentially explaining the diversity of disease phenotypes.

In addition to forming the pore, the NT, TM1, and E1 domains have been shown to be important in voltage-dependent gating and regulation of hemichannels. In fact, some pore-lining residues appear to participate in the gating process. In Cx50 hemichannels, cysteine substitutions at two pore-lining positions, F43 and G46, equivalent to positions E42 and G45 in Cx26, resulted in hemichannel lock-up because of the formation of a high affinity site for coordination of heavy metals (Verselis et al., 2009). Lockup was promoted upon hyperpolarization and/or elevation of extracellular Ca^{2+}, suggesting that the TM1/E1 region moves during hemichannel closure such that the residues move to a position where they participate in metal coordination. A similar result was observed for a chimeric hemichannel, Cx32*43E1 (Tang et al., 2009). Here we observed lock-up with the G45C substitution in Cx26, suggesting that the general conformational changes that accompany hemichannel closure with hyperpolarization and/or extracellular Ca^{2+} are conserved among connexins. Closure of hemichannels by membrane hyperpolarization and extracellular Ca^{2+} has been ascribed to a mechanism provisionally called loop gating, one of two gating mechanisms present in connexin channels and hemichannels (Bukauskas et al., 1995; Trexler et al., 1996; Oh et al., 2000; Bukauskas and Verselis, 2004; Srinivas et al., 2005). Loop gating has been shown to be an intrinsic voltage-dependent mechanism that is selectivity modulated by extracellular divalent cations, which act to stabilize the fully closed conformation and to shift activation along the voltage axis (Verselis and Srinivas, 2008). Closure on depolarization occurs through a separate gating mechanism that is insensitive to extracellular Ca^{2+} and gates hemichannels to a subconducting state (Trexler et al., 1996; Verselis and Srinivas, 2008). Although G45E hemichannels do exhibit an increase in voltage sensitivity, it is mainly at positive voltages exceeding 30 mV that, perhaps, would be relevant only in excitable cells.

Our data suggest that the A40 position is not pore lining and that the A40V substitution considerably weakens regulation of the hemichannel by extracellular Ca^{2+}. The fact that MTS reagents exhibited effects on macroscopic A40C currents suggests that the cysteine side chain may be accessible, at least from the extracellular side, albeit not readily because of the considerably slower kinetics. Regardless of the MTS reagent, the effect was the same, namely a reduction in the magnitude of the current. Collectively with the effect of the A40V substitution on Ca^{2+} regulation, modifications at the A40 position may

lead to changes in hemichannel gating and perhaps indirect changes in unitary conductance, although we did not observe the latter upon MTS application.

Studies in Cx32 hemichannels have suggested that the binding site for extracellular Ca^{2+} is formed by Asp residues D169 and D178 in the second extracellular loop domain, E2; substitution of Asn for Asp at either position nearly abolished Ca^{2+} sensitivity (Gómez-Hernández et al., 2003). However, Cx26 has a naturally occurring Asn at position 170 (equivalent to 169 in Cx32), yet is more sensitive to Ca^{2+} than is WT Cx32. Also, domain exchange between Cx46 and Cx50 indicates that the difference in Ca^{2+} regulation exhibited for these two highly sensitive connexins segregates with the N-terminal half of the connexin protein, excluding E2, suggesting that E1 likely contains the Ca^{2+}-binding site (Srinivas et al., 2006; Verselis and Srinivas, 2008). Ca^{2+}-binding sites usually consist of acidic residues that contribute carboxylate oxygens. Thus, although A40 is unlikely to constitute the Ca^{2+}-binding site, the effect of the A40V mutation likely results from a local perturbation in E1 structure that, in turn, alters Ca^{2+} binding. Other mutations in E1 that cause syndromic deafness include N54K/H, G59A/S/R, D66H, and H73R. Interestingly, several of these are charge substitutions. Extracellular Ca^{2+} does play a key role in normal epidermal differentiation, regulating the processes of cell proliferation, terminal differentiation, and cell–cell adhesion (Hennings et al., 1980; Bikle et al., 2004; Tu et al., 2004). In addition, altered calcium regulation has been implicated in the pathogenesis of some epidermal diseases (Fairley, 1991). Changes in the extracellular Ca^{2+} concentration are thought to promote the developmental switch from keratinocyte proliferation to terminal differentiation by providing a reservoir of Ca^{2+} ions that influence intracellular calcium–dependent signaling processes. In this regard, the phenotypes of reduced calcium gating (A40V) and increased calcium permeability (G45E) could both profoundly affect epidermal homeostasis.

The case for hemichannel gain of function in KID

Several lines of evidence argue that the phenotypes observed in patients carrying G45E or A40V mutations are the result of hemichannel gain of function. First, both mutants function as gap junction (cell–cell) channels. Although electrically functional as gap junction channels, it is possible that G45E and A40V behave as loss-of-function mutants as a result of loss in the ability to transfer important signaling molecules or metabolites (Beltramello et al., 2005; Zhang et al., 2005). However, loss of Cx26 gap junction channel function is only associated with deafness, not skin disorders. Also, given that G45E points into the lumen of the pore and alters pore properties, whereas A40V does not, it is unlikely that both mutations would cause the same effect on hemichannel permeability. The latter also argues against a gap junction channel gain of function as a likely explanation. Finally, cochlear development was not affected by loss of Cx26 in a mouse model, although there was some cell death in the Organ of Corti (Cohen-Salmon et al., 2002). Thus, Cx26 gap junctions do not appear to be vital for development of the cochlea but rather are involved in generating the endocochlear potential that is essential for sensory transduction by hair cells (Cohen-Salmon et al., 2002) or in providing coupling of metabolites and/or signaling molecules (Beltramello et al., 2005). In a study that examined tissue from a deceased infant with KID syndrome carrying the G45E mutation, there was cochleosaccular dysplasia and widespread abnormalities in stria vascularis as well as Reissner's and tectorial membranes (Griffith et al., 2006). In skin, the fatal septicemia likely resulted from defects in cutaneous barrier function. Thus, the pathologies both in the cochlea and skin observed with G45E are indicative of widespread cellular dysfunction, which is plausibly explained by having aberrant hemichannels in the membrane through which vital cellular contents can be lost and/or detrimental ions, such as Ca^{2+}, can gain entry.

Summary

Here we examined two mutations that cause syndromic deafness associated with severe forms of KID. We find that increased hemichannel activity caused by dysregulation by Ca^{2+} is likely the principal mechanism that contributes to disease in the case of A40V. However, in the case of G45E, which is a pore-lining position, altered permeability leading to increased Ca^{2+} entry may be a significant contributor. Finally, we find that WT Cx26 hemichannels themselves are Ca^{2+} permeable and could potentially function in Ca^{2+} signaling. The end result for both mutations may be similar: rundown of the membrane potential, excessive Ca^{2+} entry, and loss of metabolites leading to cell dysfunction or even death.

We wish to thank C. Rubinos for technical assistance.

This work was supported by National Institutes of Health grants AR059505 to T.W. White and GM54179 to V.K. Verselis.

Angus C. Nairn served as editor.

Submitted: 11 March 2010
Accepted: 9 June 2010

REFERENCES

Barish, M.E. 1983. A transient calcium-dependent chloride current in the immature *Xenopus* oocyte. *J. Physiol.* 342:309–325.

Beltramello, M., V. Piazza, F.F. Bukauskas, T. Pozzan, and F. Mammano. 2005. Impaired permeability to Ins(1,4,5)P3 in a mutant connexin underlies recessive hereditary deafness. *Nat. Cell Biol.* 7:63–69. doi:10.1038/ncb1205

Bikle, D.D., S. Chang, D. Crumrine, H. Elalieh, M.Q. Man, O. Dardenne, Z. Xie, R.S. Arnaud, K. Feingold, and P.M. Elias. 2004. Mice lacking 25OHD 1alpha-hydroxylase demonstrate decreased epidermal differentiation and barrier function. *J. Steroid Biochem. Mol. Biol.* 89-90:347–353. doi:10.1016/j.jsbmb.2004.03.113

Bukauskas, F.F., and V.K. Verselis. 2004. Gap junction channel gating. *Biochim. Biophys. Acta.* 1662:42–60. doi:10.1016/j.bbamem.2004.01.008

Bukauskas, F.F., C. Elfgang, K. Willecke, and R. Weingart. 1995. Biophysical properties of gap junction channels formed by mouse connexin40 in induced pairs of transfected human HeLa cells. *Biophys. J.* 68:2289–2298. doi:10.1016/S0006-3495(95)80411-X

Cohen-Salmon, M., T. Ott, V. Michel, J.P. Hardelin, I. Perfettini, M. Eybalin, T. Wu, D.C. Marcus, P. Wangemann, K. Willecke, and C. Petit. 2002. Targeted ablation of connexin26 in the inner ear epithelial gap junction network causes hearing impairment and cell death. *Curr. Biol.* 12:1106–1111. doi:10.1016/S0960-9822(02)00904-1

De Vuyst, E., E. Decrock, L. Cabooter, G.R. Dubyak, C.C. Naus, W.H. Evans, and L. Leybaert. 2006. Intracellular calcium changes trigger connexin 32 hemichannel opening. *EMBO J.* 25:34–44. doi:10.1038/sj.emboj.7600908

Fairley, J.A. 1991. Calcium metabolism and the pathogenesis of dermatologic disease. *Semin. Dermatol.* 10:225–231.

Gerido, D.A., and T.W. White. 2004. Connexin disorders of the ear, skin, and lens. *Biochim. Biophys. Acta.* 1662:159–170. doi:10.1016/j.bbamem.2003.10.017

Gerido, D.A., A.M. DeRosa, G. Richard, and T.W. White. 2007. Aberrant hemichannel properties of Cx26 mutations causing skin disease and deafness. *Am. J. Physiol. Cell Physiol.* 293:C337–C345. doi:10.1152/ajpcell.00626.2006

Goldberg, G.S., V. Valiunas, and P.R. Brink. 2004. Selective permeability of gap junction channels. *Biochim. Biophys. Acta.* 1662:96–101. doi:10.1016/j.bbamem.2003.11.022

Gómez-Hernández, J.M., M. de Miguel, B. Larrosa, D. González, and L.C. Barrio. 2003. Molecular basis of calcium regulation in connexin-32 hemichannels. *Proc. Natl. Acad. Sci. USA.* 100:16030–16035. doi:10.1073/pnas.2530348100

González, D., J.M. Gómez-Hernández, and L.C. Barrio. 2006. Species specificity of mammalian connexin-26 to form open voltage-gated hemichannels. *FASEB J.* 20:2329–2338. doi:10.1096/fj.06-5828com

Griffith, A.J., Y. Yang, S.P. Pryor, H.J. Park, E.W. Jabs, J.B. Nadol Jr., L.J. Russell, D.I. Wasserman, G. Richard, J.C. Adams, and S.N. Merchant. 2006. Cochleosaccular dysplasia associated with a connexin 26 mutation in keratitis-ichthyosis-deafness syndrome. *Laryngoscope.* 116:1404–1408. doi:10.1097/01.mlg.0000224549.75161.ca

Harris, A.L. 2001. Emerging issues of connexin channels: biophysics fills the gap. *Q. Rev. Biophys.* 34:325–472.

Hennings, H., D. Michael, C. Cheng, P. Steinert, K. Holbrook, and S.H. Yuspa. 1980. Calcium regulation of growth and differentiation of mouse epidermal cells in culture. *Cell.* 19:245–254. doi:10.1016/0092-8674(80)90406-7

Hoang Dinh, E., S. Ahmad, Q. Chang, W. Tang, B. Stong, and X. Lin. 2009. Diverse deafness mechanisms of connexin mutations revealed by studies using in vitro approaches and mouse models. *Brain Res.* 1277:52–69. doi:10.1016/j.brainres.2009.02.008

Horton, R.M., Z.L. Cai, S.N. Ho, and L.R. Pease. 1990. Gene splicing by overlap extension: tailor-made genes using the polymerase chain reaction. *Biotechniques.* 8:528–535.

Janecke, A.R., H.C. Hennies, B. Gunther, G. Gansl, J. Smolle, E.M. Messmer, G. Utermann, and O. Rittinger. 2005. GJB2 mutations in keratitis-ichthyosis-deafness syndrome including its fatal form. *Am. J. Med. Genet. A.* 133A:128–131.

Karlin, A., and M.H. Akabas. 1998. Substituted-cysteine accessibility method. *Methods Enzymol.* 293:123–145. doi:10.1016/S0076-6879(98)93011-7

Kelsell, D.P., J. Dunlop, H.P. Stevens, N.J. Lench, J.N. Liang, G. Parry, R.F. Mueller, and I.M. Leigh. 1997. Connexin 26 mutations in hereditary non-syndromic sensorineural deafness. *Nature.* 387:80–83. doi:10.1038/387080a0

Kronengold, J., E.B. Trexler, F.F. Bukauskas, T.A. Bargiello, and V.K. Verselis. 2003a. Pore-lining residues identified by single channel SCAM studies in Cx46 hemichannels. *Cell Commun. Adhes.* 10:193–199.

Kronengold, J., E.B. Trexler, F.F. Bukauskas, T.A. Bargiello, and V.K. Verselis. 2003b. Single-channel SCAM identifies pore-lining residues in the first extracellular loop and first transmembrane domains of Cx46 hemichannels. *J. Gen. Physiol.* 122:389–405. doi:10.1085/jgp.200308861

Kuruma, A., and H.C. Hartzell. 1999. Dynamics of calcium regulation of chloride currents in *Xenopus* oocytes. *Am. J. Physiol.* 276:C161–C175.

Lai-Cheong, J.E., K. Arita, and J.A. McGrath. 2007. Genetic diseases of junctions. *J. Invest. Dermatol.* 127:2713–2725. doi:10.1038/sj.jid.5700727

Lang, F., V. Vallon, M. Knipper, and P. Wangemann. 2007. Functional significance of channels and transporters expressed in the inner ear and kidney. *Am. J. Physiol. Cell Physiol.* 293:C1187–C1208. doi:10.1152/ajpcell.00024.2007

Lee, J.R., and T.W. White. 2009. Connexin-26 mutations in deafness and skin disease. *Expert Rev. Mol. Med.* 11:e35. doi:10.1017/S1462399409001276

Lee, J.R., A.M. Derosa, and T.W. White. 2009. Connexin mutations causing skin disease and deafness increase hemichannel activity and cell death when expressed in *Xenopus* oocytes. *J. Invest. Dermatol.* 129:870–878. doi:10.1038/jid.2008.335

Maeda, S., S. Nakagawa, M. Suga, E. Yamashita, A. Oshima, Y. Fujiyoshi, and T. Tsukihara. 2009. Structure of the connexin 26 gap junction channel at 3.5 A resolution. *Nature.* 458:597–602. doi:10.1038/nature07869

Meşe, G., V. Valiunas, P.R. Brink, and T.W. White. 2008. Connexin26 deafness associated mutations show altered permeability to large cationic molecules. *Am. J. Physiol. Cell Physiol.* 295:C966–C974. doi:10.1152/ajpcell.00008.2008

Montgomery, J.R., T.W. White, B.L. Martin, M.L. Turner, and S.M. Holland. 2004. A novel connexin 26 gene mutation associated with features of the keratitis-ichthyosis-deafness syndrome and the follicular occlusion triad. *J. Am. Acad. Dermatol.* 51:377–382. doi:10.1016/j.jaad.2003.12.042

Oesterle, E.C., and P. Dallos. 1990. Intracellular recordings from supporting cells in the guinea pig cochlea: DC potentials. *J. Neurophysiol.* 64:617–636.

Oh, S., J.B. Rubin, M.V. Bennett, V.K. Verselis, and T.A. Bargiello. 1999. Molecular determinants of electrical rectification of single channel conductance in gap junctions formed by connexins 26 and 32. *J. Gen. Physiol.* 114:339–364. doi:10.1085/jgp.114.3.339

Oh, S., C.K. Abrams, V.K. Verselis, and T.A. Bargiello. 2000. Stoichiometry of transjunctional voltage-gating polarity reversal by a negative charge substitution in the amino terminus of a connexin32 chimera. *J. Gen. Physiol.* 116:13–31. doi:10.1085/jgp.116.1.13

Purnick, P.E., D.C. Benjamin, V.K. Verselis, T.A. Bargiello, and T.L. Dowd. 2000a. Structure of the amino terminus of a gap junction protein. *Arch. Biochem. Biophys.* 381:181–190. doi:10.1006/abbi.2000.1989

Purnick, P.E., S. Oh, C.K. Abrams, V.K. Verselis, and T.A. Bargiello. 2000b. Reversal of the gating polarity of gap junctions by negative charge substitutions in the N-terminus of connexin 32. *Biophys. J.* 79:2403–2415. doi:10.1016/S0006-3495(00)76485-X

Richard, G. 2000. Connexins: a connection with the skin. *Exp. Dermatol.* 9:77–96. doi:10.1034/j.1600-0625.2000.009002077.x

Richard, G. 2001. Human connexin disorders of the skin. *Cell Commun. Adhes.* 8:401–407. doi:10.3109/15419060109080761

Richard, G., L.E. Smith, R.A. Bailey, P. Itin, D. Hohl, E.H. Epstein Jr., J.J. DiGiovanna, J.G. Compton, and S.J. Bale. 1998. Mutations in the human connexin gene GJB3 cause erythrokeratodermia variabilis. *Nat. Genet.* 20:366–369. doi:10.1038/3840

Richard, G., F. Rouan, C.E. Willoughby, N. Brown, P. Chung, M. Ryynänen, E.W. Jabs, S.J. Bale, J.J. DiGiovanna, J. Uitto, and L. Russell. 2002. Missense mutations in GJB2 encoding connexin-26 cause the ectodermal dysplasia keratitis-ichthyosis-deafness syndrome. *Am. J. Hum. Genet.* 70:1341–1348. doi:10.1086/339986

Rouan, F., T.W. White, N. Brown, A.M. Taylor, T.W. Lucke, D.L. Paul, C.S. Munro, J. Uitto, M.B. Hodgins, and G. Richard. 2001. trans-dominant inhibition of connexin-43 by mutant connexin-26: implications for dominant connexin disorders affecting epidermal differentiation. *J. Cell Sci.* 114:2105–2113.

Sánchez, H.A., J.A. Orellana, V.K. Verselis, and J.C. Sáez. 2009. Metabolic inhibition increases activity of connexin-32 hemichannels permeable to Ca2+ in transfected HeLa cells. *Am. J. Physiol. Cell Physiol.* 297:C665–C678. doi:10.1152/ajpcell.00200.2009

Schalper, K.A., N. Palacios-Prado, M.A. Retamal, K.F. Shoji, A.D. Martínez, and J.C. Sáez. 2008. Connexin hemichannel composition determines the FGF-1-induced membrane permeability and free [Ca2+]i responses. *Mol. Biol. Cell.* 19:3501–3513. doi:10.1091/mbc.E07-12-1240

Srinivas, M., J. Kronengold, F.F. Bukauskas, T.A. Bargiello, and V.K. Verselis. 2005. Correlative studies of gating in Cx46 and Cx50 hemichannels and gap junction channels. *Biophys. J.* 88:1725–1739. doi:10.1529/biophysj.104.054023

Srinivas, M., D.P. Calderon, J. Kronengold, and V.K. Verselis. 2006. Regulation of connexin hemichannels by monovalent cations. *J. Gen. Physiol.* 127:67–75. doi:10.1085/jgp.200509397

Stong, B.C., Q. Chang, S. Ahmad, and X. Lin. 2006. A novel mechanism for connexin 26 mutation linked deafness: cell death caused by leaky gap junction hemichannels. *Laryngoscope.* 116:2205–2210. doi:10.1097/01.mlg.0000241944.77192.d2

Suchyna, T.M., J.M. Nitsche, M. Chilton, A.L. Harris, R.D. Veenstra, and B.J. Nicholson. 1999. Different ionic selectivities for connexins 26 and 32 produce rectifying gap junction channels. *Biophys. J.* 77:2968–2987. doi:10.1016/S0006-3495(99)77129-8

Tang, Q., T.L. Dowd, V.K. Verselis, and T.A. Bargiello. 2009. Conformational changes in a pore-forming region underlie voltage-dependent "loop gating" of an unapposed connexin hemichannel. *J. Gen. Physiol.* 133:555–570. doi:10.1085/jgp.200910207

Terrinoni, A., A. Codispoti, V. Serra, E. Bruno, B. Didona, M. Paradisi, S. Nisticò, E. Campione, B. Napolitano, L. Diluvio, and G. Melino. 2010a. Connexin 26 (GJB2) mutations as a cause of the KID syndrome with hearing loss. *Biochem. Biophys. Res. Commun.* 395:25–30. doi:10.1016/j.bbrc.2010.03.098

Terrinoni, A., A. Codispoti, V. Serra, B. Didona, E. Bruno, R. Nisticò, M. Giustizieri, M. Alessandrini, E. Campione, and G. Melino. 2010b. Connexin 26 (GJB2) mutations, causing KID Syndrome, are associated with cell death due to calcium gating deregulation. *Biochem. Biophys. Res. Commun.* 394:909–914. doi:10.1016/j.bbrc.2010.03.073

Trexler, E.B., M.V. Bennett, T.A. Bargiello, and V.K. Verselis. 1996. Voltage gating and permeation in a gap junction hemichannel. *Proc. Natl. Acad. Sci. USA.* 93:5836–5841. doi:10.1073/pnas.93.12.5836

Trexler, E.B., F.F. Bukauskas, J. Kronengold, T.A. Bargiello, and V.K. Verselis. 2000. The first extracellular loop domain is a major determinant of charge selectivity in connexin46 channels. *Biophys. J.* 79:3036–3051. doi:10.1016/S0006-3495(00)76539-8

Tu, C.L., Y. Oda, L. Komuves, and D.D. Bikle. 2004. The role of the calcium-sensing receptor in epidermal differentiation. *Cell Calcium.* 35:265–273. doi:10.1016/j.ceca.2003.10.019

van Steensel, M.A., M. van Geel, M. Nahuys, J.H. Smitt, and P.M. Steijlen. 2002. A novel connexin 26 mutation in a patient diagnosed with keratitis-ichthyosis-deafness syndrome. *J. Invest. Dermatol.* 118:724–727. doi:10.1046/j.1523-1747.2002.01735.x

Verselis, V.K. 2009. The connexin channel pore: pore-lining segments and residues. *In* Connexins: A Guide. A. Harris and D. Locke, editors. Humana Press, New York. 77–102.

Verselis, V.K., and M. Srinivas. 2008. Divalent cations regulate connexin hemichannels by modulating intrinsic voltage-dependent gating. *J. Gen. Physiol.* 132:315–327. doi:10.1085/jgp.200810029

Verselis, V.K., and R.D. Veenstra. 2000. Gap junction channels: permeability and voltage gating. *In* Gap Junctions. Vol. 30. E.L. Hertzberg, editor. JAI Press, Stamford, CT. 129–192.

Verselis, V.K., C.S. Ginter, and T.A. Bargiello. 1994. Opposite voltage gating polarities of two closely related connexins. *Nature.* 368:348–351. doi:10.1038/368348a0

Verselis, V.K., M.P. Trelles, C. Rubinos, T.A. Bargiello, and M. Srinivas. 2009. Loop gating of connexin hemichannels involves movement of pore-lining residues in the first extracellular loop domain. *J. Biol. Chem.* 284:4484–4493. doi:10.1074/jbc.M807430200

Wilders, R., and H.J. Jongsma. 1992. Limitations of the dual voltage clamp method in assaying conductance and kinetics of gap junction channels. *Biophys. J.* 63:942–953. doi:10.1016/S0006-3495(92)81664-8

Wohlrab, D., J. Wohlrab, and F. Markwardt. 2000. Electrophysiological characterization of human keratinocytes using the patch-clamp technique. *Exp. Dermatol.* 9:219–223. doi:10.1034/j.1600-0625.2000.009003219.x

Yotsumoto, S., T. Hashiguchi, X. Chen, N. Ohtake, A. Tomitaka, H. Akamatsu, K. Matsunaga, S. Shiraishi, H. Miura, J. Adachi, and T. Kanzaki. 2003. Novel mutations in GJB2 encoding connexin-26 in Japanese patients with keratitis-ichthyosis-deafness syndrome. *Br. J. Dermatol.* 148:649–653. doi:10.1046/j.1365-2133.2003.05245.x

Zhang, Y., W. Tang, S. Ahmad, J.A. Sipp, P. Chen, and X. Lin. 2005. Gap junction-mediated intercellular biochemical coupling in cochlear supporting cells is required for normal cochlear functions. *Proc. Natl. Acad. Sci. USA.* 102:15201–15206. doi:10.1073/pnas.0501859102

Zhou, X.W., A. Pfahnl, R. Werner, A. Hudder, A. Llanes, A. Luebke, and G. Dahl. 1997. Identification of a pore lining segment in gap junction hemichannels. *Biophys. J.* 72:1946–1953. doi:10.1016/S0006-3495(97)78840-4